Carbazole-based material: synthesis, characterization, and application as hole transporting material in perovskite solar cells

Diego Magaldi[1] · Maria Ulfa[2] · Sébastien Péralta[1] · Fabrice Goubard[1] · Thierry Pauporté[2] · Thanh-Tuân Bui[1]

Abstract

The synthesis and characterization of a novel oligomeric cyclic carbazole-based material (PCz1) for an application as hole transporter (HTM) in hybrid perovskite photovoltaic devices are reported. Its preliminary application in $Cs_{0.08}FA_{0.80}MA_{0.12}Pb(I_{0.88}Br_{0.12})_3$ mixed perovskite solar cell (PSC) leads to a device power conversion efficiency of 18.04% which is comparable to that of the Spiro-OMeTAD reference cells (17.94%). In addition, the novel HTM is proved to act as a good barrier and protect satisfactorily the perovskite surface giving highly stable PSC devices.

1 Introduction

Generally, the active component of a perovskite solar cell (PSC), composed of an inorganic or hybrid perovskite material layer acting as the light absorber, is sandwiched between two charge transporting layers. The hole transporting layer (HTL) extracts holes at the HTL/perovskite interface and transports them towards the cathode while the electron transporting layer (ETL) permits the electrons extraction and transportation. It has been clearly established that the incorporation of HTL and ETL in PSC's device structure is highly important for the devices to be efficient and stable [1]. In this context, accurate design of HTL is of major interest. The HTL is usually made from a single hole transporting material (HTM). However, in some cases, a mixture of different HTM can be employed. [2] Hole transporting capacity is key for achieving high photovoltaic efficiency. Usually, some additives and/or chemical dopants are incorporated to increase the charge transport capacity of the organic semiconductors. In addition, the E_{HOMO} and E_{LUMO} of the HTM must be compatible with the valence band maximum and conduction band minimum of the perovskite in order to provide the suitable driving force for charge transfer and block the electrons' back transfer. Other researched characteristics include excellent thermal, morphological, and photochemical stability, and good hydrophobic properties to protect the perovskite materials from moisture. The hole transporter can be either inorganic, organic, or coordination compounds [3, 4]. Organic HTMs are subclassified into molecular and polymeric materials. If molecular HTMs have well-defined molecular weight and structure and good synthetic reproducibility, the polymeric counterparts have important advantages in terms of processability, thermal and mechanical stability, and higher intrinsic hole mobility [5] Among various organic HTM, carbazole-based HTMs is of particular interest thanks to their unique features suitable for developing photovoltaic materials [6, 7, 16–25, 8–15]. We have previously exploited carbazole platform to design HTMs for solid-state DSSCs [9] and PSCs. [6, 11, 26]. Bulky dendritic carbazole compound, which take the best of both molecular and polymeric HTMs features, has been proved to be an effective design strategy, giving improved PSCs in terms of the stability [6, 7]. Herein, a new oligomeric cyclic carbazole-based HTM (Scheme 1) is proposed which provide device performance comparable to that of Spiro-OMeTAD and also markedly improves the device stability.

The presence of the 2,4,6-trimethylaniline unit as hydrophobic and structuring agent is expected to favor the nano-structuration in HTM inducing a better conductivity in PSC device. This singularity has already been observed with PTAA as HTM in PSCs. [27] Moreover,

✉ Thanh-Tuân Bui
  tbui@cyu.fr

[1] CY Cergy Paris Université, LPPI, F-95000 Cergy, France

[2] Chimie ParisTech, PSL Research University, CNRS, Institut de Recherche de Chimie Paris (IRCP- UMR8247), 11 rue P. et M. Curie, F-75005 Paris, France
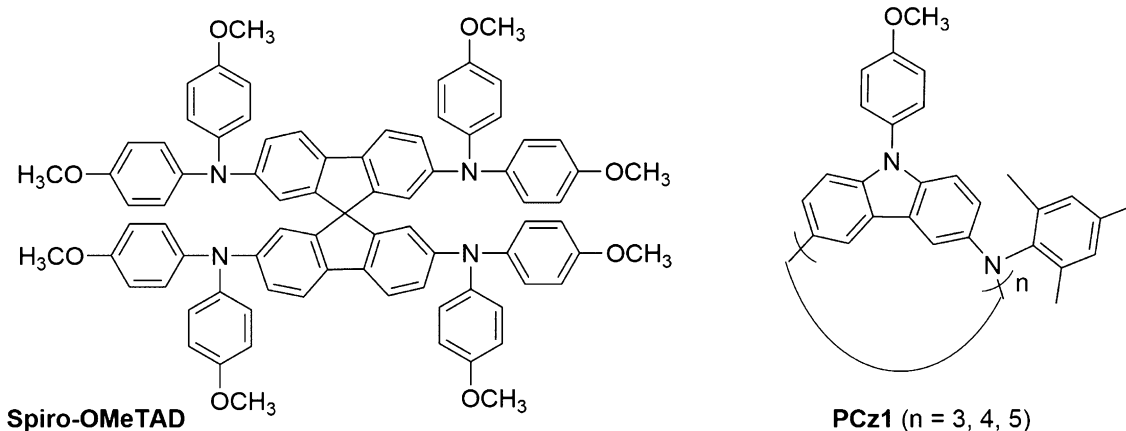
**Scheme 1** Molecular structures of investigated HTMs

methyl groups decrease the arrangement disorder between molecules due to lower repulsion of methyl groups and benzene rings, favoring also the carrier mobility within the HTM. [28].

2 Results and discussion

2.1 Material synthesis

PCz1 was synthetized in three steps as detailed in Scheme 2. Briefly, *N*-(4-methoxyphenyl)carbazole (**1**) was produced by a copper-catalyzed Ullmann amination reaction. **1** was then

Scheme 2 Synthesis of carbazole-based HTM **PCz1**
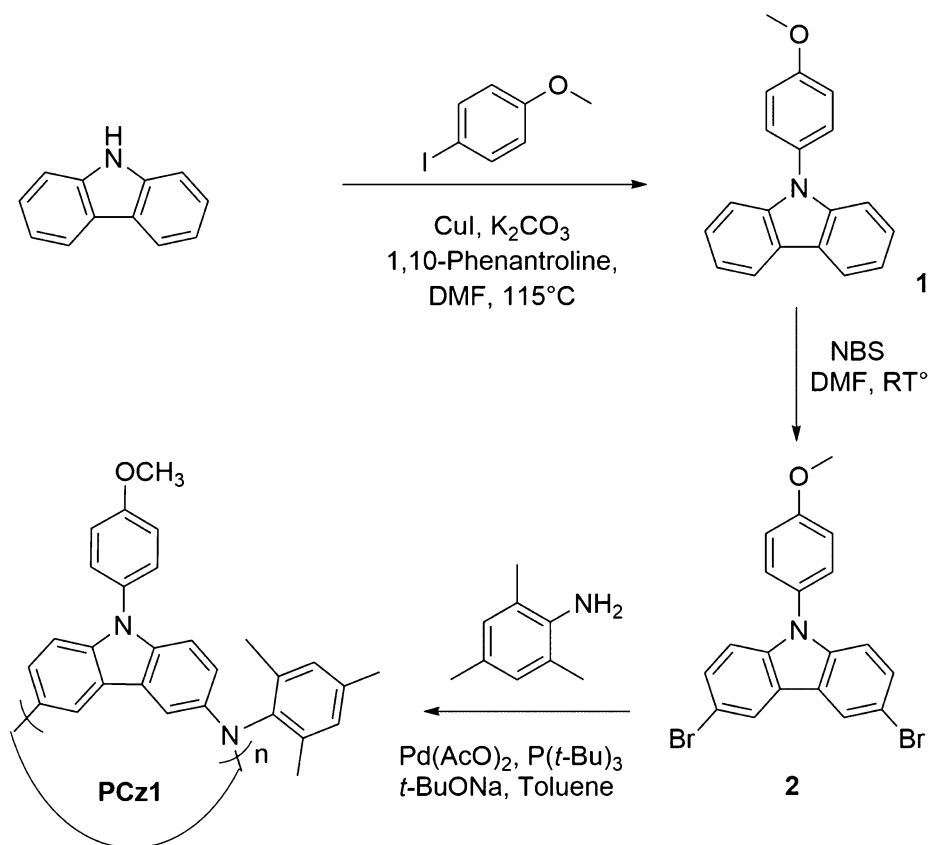
treated by *N*-bromosuccinimide giving 3,6-dibromo-*N*-(4-methoxyphenyl)carbazole (**2**).

The final step consisted in a Pd-catalyzed Buchwald Hartwig amination reaction. The treatment of **2** with an equimolar equivalence of 2,4,6-triphenylaniline gave an inseparable mixture of oligomers. MALDI-TOF MS analysis suggests clearly the co-existence of tris-, tetra-. and penta-co-oligomers in the mixture. The theoretical DFT calculations have confirmed the presence of a mixture of different oligomers in the mixture. The obtained materials presented a good solubility in organic solvents commonly used for the deposition of HTM such as chlorobenzene, toluene, chloroform, etc. We then directly characterized this mixture for the purpose of application as HTM in PSCs.

# 3 Material characterization

3.1 DFT calculation

These oligomers (tris-, tetra-, and penta-cyclic compounds) were investigated by DFT. The optimized geometries and

energies of the tetra-oligomer, the most abundant one, are given in the Fig. 1 and the data for the other two compounds are provided in the ESI (Figures S1, S2, and Table S1).

As can be observed for **PCz1**, their HOMO and LUMO were partially developed over the whole molecular structure. This is explained by the fact that the cyclic compounds have a distorted structure. All oligomers have nearly an identical optimized energy per repeated unit (Table S1, ESI). While the E_{LUMO} levels are nearly identical for all the compounds, the tris-oligomer has a deeper HOMO level compared to the tetra and penta oligomers.

3.2 Thermal, morphological, and optoelectrochemical properties

PCz1 showed a good thermal stability with a $T_d > 340$ °C (Fig. 2a) which is high enough for the applications in PSC. No melting point was observed until 280 °C in differential scanning calorimetry (DSC) analysis (data not shown) suggesting that the material obtained is amorphous. However, the DSC curves revealed a complex behavior due to the presence of different oligomers.
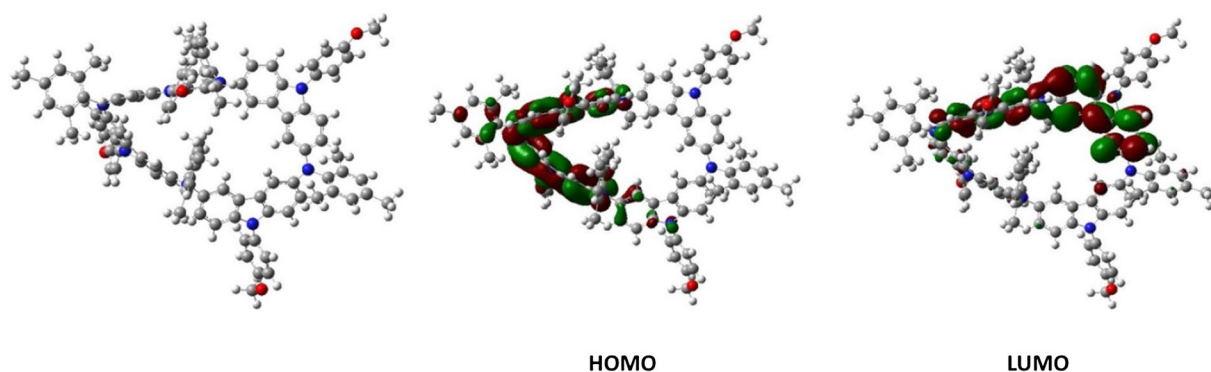
HOMO   LUMO

Fig. 1 Optimized geometry and HOMO LUMO distribution of the tetra-oligomer
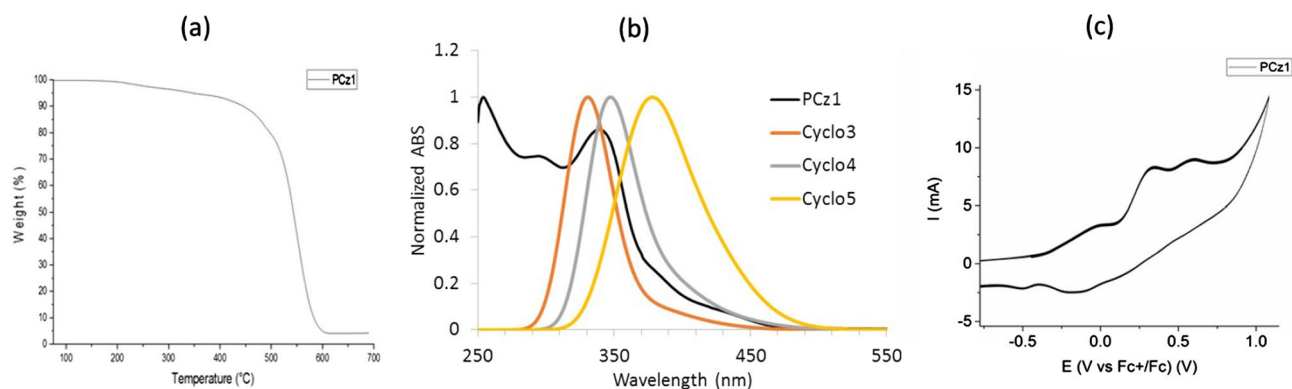
Fig. 2 **a** TGA curve of **PCz1**. **b** Absorbance of **PCz1** in dichloromethane and calculated spectra for tris, tetra and penta cyclic molecules (Cyclo*N*, *N* = 3, 4 and 5). **c** Cyclic voltammetry of **PCz1** in dichloromethane

The absorption properties of the **PCz1** mixture recorded in dilute dichloromethane solution are shown in Fig. 2b. It presents a strong absorption band centered at 338 nm and shoulders at lower energy attributed to an extended conjugated system including carbazole/tertiary amine ones. The simulated absorption spectra in CH_2Cl_2 of different oligomers are also displayed in Fig. 2b with the maximum absorption wavelength of 331, 347, and 378 nm for tris-, tetra-, and penta-cyclic molecules, respectively. This is in good accordance with the assumption that **PCz1** is a mixture composed mainly of these cyclic oligomers. **PCz1** mainly absorbs in the UV spectral domain, which will not cause a competitive absorption effect with the perovskite materials. The optical bandgap ($E_g = 2.74$ eV) is calculated from the absorption onset wavelength (Fig. 2b and 460 nm). This value is somewhat smaller than that of the Spiro-OMeTAD (3.00 eV).[9] Cyclic voltammetry (CV) was employed to investigate the redox behavior of **PCz1** in dilute solution (Fig. 2c). The cyclic voltammogram of **PCz1** shows multiple oxidation processes. The first reversible oxidation could be attributed to the formation of radical cation of the carbazole moiety. **PCz1** has an oxidation onset potential of -0.36 V *versus* Fc/Fc$^+$, which is lower than that of **Spiro-OMeTAD** (-0.11 V/ Fc/Fc$^+$) measured under the same conditions. [9] These redox potentials were then employed to estimate their E_{HOMO} and E_{LUMO} in the solid state by using the ferrocene ionization energy as the standard. E_{HOMO} was estimated from the first oxidation potential while E_{LUMO} was estimated from the E_{HOMO} and E_g. The E_{HOMO} values of **PCz1** and **Spiro-OMeTAD** are -4.74 eV and -4.99 eV, respectively, assuming that the ionization potential of Ferrocene is 5.1 eV versus vacuum. The corresponding E_{LUMO} values are -2.0 and -1.99 eV, respectively. The E_{HOMO} level of **PCz**1 is thus higher than that of Spiro-OMeTAD meanwhile both compounds have very similar E_{LUMO} levels. This suggests that, energetically, **PCz1** could be suitable as an alternative HTM to **Spiro-OMeTAD**.

In order to improve the device stability against moisture in real operation, the HTM layer must protect the perovskite layer as far as possible. Hydrophilic HTM will be more susceptible to moisture ingress than the hydrophobic ones. Even if the permeability to liquid water/moisture can also depend on other factors such as thin film porosity, it remains that hydrophobicity should play a key role in moisture resistance for films of similar smoothness and compactness. We performed water contact angle measurements on the **PCz1** layers studied in this work. LiTFSI and *tert* butylpyridine were incorporated into the film for mimicking the condition in PSCs. **PCz1** film exhibited an average contact angle value of $93.7 \pm 5.6°$, which corresponds to rather high hydrophobic properties compared to Spiro-OMeTAD (70°) (Figure S3 in ESI) [29]. It has been demonstrated that such hydrophobic properties are extremely beneficial to PSC stability [30]. A low surface roughness is an important requirement to decrease the current losses in PSC and get a better contact with the counter-electrode. For this purpose, the film forming property of doped **PCz1** was examined by atomic force microscopy (Figure S4 in ESI). The **PCz1** film showed a uniform and smooth surface with a mean surface roughness values of 0.97 nm. This low value should improve the contact with the perovskite layer and counter-electrode.

3.3 Photovoltaic application

PCz1 was then studied as HTMs using $Cs_{0.08}FA_{0.80}MA_{0.12}Pb(I_{0.88}Br_{0.12})_3$ perovskite as the absorber material which has proved to be highly efficient for PSC application [31, 32]. The device structure employed was as follows: Glass-FTO/cTiO$_2$/mpTiO$_2$/perovskite/HTM/Au with cTiO$_2$ a compact layer prepared by spray pyrolysis and mpTiO$_2$ a mesoporous TiO$_2$ layer prepared by spin coating [33, 34]. As mentioned above, the E_{HOMO} and E_{LUMO} of **PCz1** are close to that of Spiro-OMeTAD so **PCz1** should be suitable and work as well as **Spiro-OMeTAD**. The best cell *J-V* curves are displayed in Fig. 3a and the *J-V* curve parameters are gathered in Table 1. The initial performances of **Spiro-OMeTAD** cells were superior to those of the **PCz1** cells. The former exhibited a better V$_{oc}$ and J$_{sc}$. Both cells had a rather large hysteresis between the reverse and the forward scan curves. This trend was observed for both the

Table 1 Photovoltaic *J-V* parameters and PCE of best PSC cells prepared with PCz1 and Spiro-OMeTAD

	HTM	Scan direction	V$_{oc}$ (V)	J$_{sc}$ (mA.cm^{-2})	FF (%)	PCE (%)	HI[b] (%)
Fresh cells	Spiro-OMeTAD	Reverse	0.99	22.25	81.20	17.94	26.9
		Forward	0.91	22.19	65.06	13.12	
	PCz1	Reverse	0.95	21.88	80.87	16.84	30.1
		Forward	0.86	21.91	62.45	11.76	
Aged cells[a]	Spiro-OMeTAD	Reverse	1.00	22.62	75.55	17.14	8.1
		Forward	1.02	22.55	68.79	15.76	
	PCz1	Reverse	1.04	22.41	77.55	18.04	32.5
		Forward	0.97	22.44	55.70	12.17	

[a] 7-week-old cells. [b] Hysteresis index defined as: $HI(\%) = \frac{PCE_{rev} - PCE_{for}}{PCE_{rev}}$

Fig. 3 *J-V* and EQE curves of PSC devices **a** *J-V* curves of **PCz1** and **Spiro-OMeTAD** cells, fresh and 7 weeks old; **b** EQE curves of **PCz1** and **Spiro-OMeTAD** cells
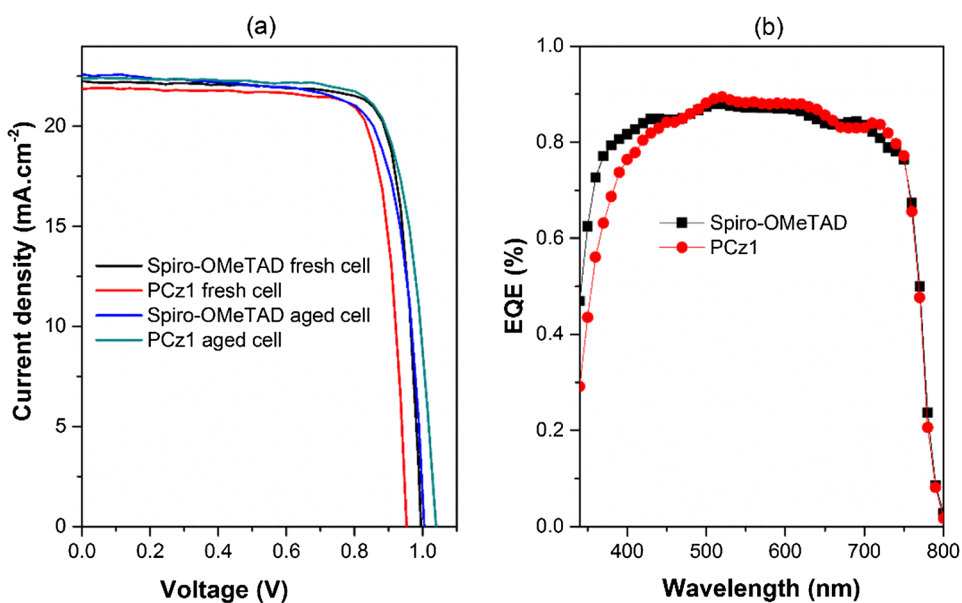
record cells and the averaged data (Table S2 in the ESI). Table 1 also reports the *J-V* curve parameters after 7 weeks of aging (storage in the N_2 filled glovebox). We remark that the efficiency of the **Spiro-OMeTAD** PSCs decreased during this period of time. On the other hand, the PCE of **PCz1** cells increased significantly reaching a value of 18.04%, which is slightly superior to the initial PCE of the **Spiro-OMeTAD** PSC. Aging reduces the hysteresis in the case of the **Spiro-OMeTAD** device, while this parameter was slightly enlarged in the case of the **PCz1** cell. Nevertheless, some of us have shown recently that with the triple cation perovskite employed in this study, the systems have a slow response in time and that the steady-state PCE is close to the PCE determined in the reverse bias scan conditions [31]. Figure 3b compares the spectral response of the two kinds of cells. The external quantum efficiency (EQE) curves of fresh cells are very close in the visible and near infra-red regions. They reach high efficiency values, up to 85%. The spectra present an edge at about 780 nm due to the bandgap of the employed perovskite (1.60 eV). The main difference is found in the UV region with **PCz1** cells having lower EQE(%) in the UV region which is related to the lower bandgap of **PCz1** compared to Spiro-OMeTAD that could reduce the component due to the light reflection on the back electrode. Nevertheless, as the UV-component of the solar spectrum is very low, this feature is not detrimental for the performances and the photogenerated J_{sc} is close for these two devices.

The aging of the devices and the stabilization of the perovskite layers and interfaces are important parameters for the development of this technology. We have followed the evolution of the *J-V* curve parameters and PCE of solar cells prepared with the two different HTMs and stored in a N_2 filled glovebox. The results are shown in Figure S5 in ESI.

Clearly, the **PCz1** cell presents a high stability with a PCE increase during the first weeks of aging. The improvement is mainly due to the enlargement of the V_{oc} and, in a less extent, of the J_{sc}. On the other hand, the Spiro-OMeTAD PSCs present stable V_{oc} and J_{sc} parameters while the FF decreases slightly. Overall, during the first 60 days, the PCE of the **PCz1** cell increased by 3% while it decreased by 5.5% for the Spiro-OMeTAD cell. It can be explained by the rather large size and flexibility of the oligomer HTM compared to the molecular one. The perovskite is covered by a denser layer and then better protected against moisture and other degrading agents. We can also suppose that the alternation of mesitylene and anisole in the **PCz1** groups allows the close packing of the molecules by the low repulsion derived of fewer methoxy groups on the molecule. The latter can be partially confirmed by the low roughness values of the deposited layer. This is in good agreement with higher hydrophobic properties of the **PCz1** film compared to the **Spiro-OMeTAD** one. The enlargement of the V_{oc} also suggests an improvement of the perovskite/PCz1 interface during the weeks following the cell preparation. Long-term stability and increment of the final PCE observed over time of 60 days are mainly due to the increase of the final voltage output from 0.98 to 1.04 V. In parallel, a small reduction of the current output going from 22.88 mA.cm^{-2} to 22.41 mA.cm^{-2} is observed. Accordingly, the final PCE went from 16.84% to 18.04% for the forward scan. It represents an increment of 7% from the first PCE measurement. Many factors can contribute to the observed phenomena like the solid-state diffusion of the different components of HTL towards its self-stabilization [35]. It is evident that the stabilization of the **PCz1** cell signifies an amelioration of the interphase contact derived of the HTL nature.

4 Conclusion

In summary, novel carbazole-based oligomers were synthetized, characterized, and applied as hole transporting material in perovskite photovoltaic devices. The thermal, morphological, optical, and electrochemical characterizations have shown that the **PCz1** oligomer material is suitable for the role of HTM. Initial photovoltaic measurements gave a PCE of 16.84% which increased over 6 weeks to reach a value of 18.04%. This PCE is superior to the PCE of the benchmark **Spiro-OMeTAD** cell. Moreover, the former has been shown much more stable than the latter. Current study is being conducted to optimize the synthesis of this family of molecules. More compounds of this family will be prepared in order to better understand the molecular structure/photovoltaic performance relationship of this series of carbazole derivatives.

5 Materials and methods

The detailed descriptions of materials synthesis, characterization, computational DFT calculation, perovskite-based photovoltaic device fabrication, and measurements are given in the Electronic Supporting Information.

Compliance with ethical standards

Conflict of interest The authors declared that they have no conflicts of interest.

References

1. H.S. Kim, I.H. Jang, N. Ahn, M. Choi, A. Guerrero, J. Bisquert, N.G. Park, J. Phys. Chem. Lett. **6**, 4633 (2015)
2. J.Y. Kim, G. Kwak, Y.C. Choi, D.H. Kim, Y.S. Han, J. Ind. Eng. Chem. **73**, 175 (2019)
3. P.K. Kung, M.H. Li, P.Y. Lin, Y.H. Chiang, C.R. Chan, T.F. Guo, P. Chen, Adv. Mater. Interfaces **5**(22), 1800882 (2018)
4. X. Zhao, M. Wang, Mater. Today Energy **7**, 208 (2018)
5. M. Ulfa, T. Zhu, F. Goubard, T. Pauporté, J. Mater. Chem. A **6**, 13350 (2018)
6. T.-T. Bui, M. Ulfa, F. Maschietto, A. Ottochian, M.-P. Nghiêm, I. Ciofini, F. Goubard, T. Pauporté, Org. Electron. **60**, 20 (2018)
7. M. Ulfa, T. Pauporte, T.-T. Bui, F. Goubard, J. Phys. Chem. C **122**, 11651 (2018)
8. T.-T. Bui, S.K. Shah, X. Sallenave, M. Abbas, G. Sini, L. Hirsch, F. Goubard, RSC Adv. **5**, 49590 (2015)
9. T.-T. Bui, S.K. Shah, M. Abbas, X. Sallenave, G. Sini, L. Hirsch, F. Goubard, ChemNanoMat **1**, 203 (2015)
10. T.T. Bui, L. Beouch, X. Sallenave, F. Goubard, Tetrahedron Lett. **54**, 4277 (2013)
11. T.-T. Bui, F. Goubard, J. Troughton, T. Watson, J. Mater. Sci. Mater. Electron. **28**, 17551 (2017)
12. A.-N. Cho, H.-S. Kim, T.-T. Bui, X. Sallenave, F. Goubard, N.-G. Park, RSC Adv. **6**, 68553 (2016)
13. Y. Xue, Y. Wu, Y. Li, J. Power Sources **344**, 160 (2017)
14. M. Daskeviciene, S. Paek, Z. Wang, T. Malinauskas, G. Jokubauskaite, K. Rakstys, K.T. Cho, A. Magomedov, V. Jankauskas, S. Ahmad, H.J. Snaith, V. Getautis, M.K. Nazeeruddin, Nano Energy **32**, 551 (2017)
15. M.-D. Zhang, B.-H. Zheng, Q.-F. Zhuang, C.-Y. Huang, H. Cao, M.-D. Chen, B. Wang, Dye. Pigment. **146**, 589 (2017)
16. K. Rakstys, S. Paek, P. Gao, P. Gratia, T. Marszalek, G. Grancini, K.T. Cho, K. Genevicius, V. Jankauskas, W. Pisula, M.K. Nazeeruddin, J. Mater. Chem. A **5**, 7811 (2017)
17. Z. Chen, H. Li, X. Zheng, Q. Zhang, Z. Li, Y. Hao, G. Fang, ChemSusChem **10**, 3111 (2017)
18. X. Yin, L. Guan, J. Yu, D. Zhao, C. Wang, N. Shrestha, Y. Han, Q. An, J. Zhou, B. Zhou, Y. Yu, C.R. Grice, R.A. Awni, F. Zhang, J. Wang, R.J. Ellingson, Y. Yan, W. Tang, Nano Energy **40**, 163 (2017)
19. Š. N. Daškevičiūtė, M. Sakai, M. Franckevičius, A. Daškevičienė, V. Magomedov, H.J. Jankauskas, Snaith, V. Getautis, Adv. Sci. 5, 1700811 (2018)
20. D. Li, J.-Y. Shao, Y. Li, Y. Li, L.-Y. Deng, Y.-W. Zhong, Q. Meng, Chem. Commun. **54**, 1651 (2018)
21. P. Gratia, A. Magomedov, T. Malinauskas, M. Daskeviciene, A. Abate, S. Ahmad, M. Grätzel, V. Getautis, M.K. Nazeeruddin, Angew. Chemie - Int. Ed. **54**, 11409 (2015)
22. A. Magomedov, S. Paek, P. Gratia, E. Kasparavicius, M. Daskeviciene, E. Kamarauskas, A. Gruodis, V. Jankauskas, K. Kantminiene, K.T. Cho, K. Rakstys, T. Malinauskas, V. Getautis, M.K. Nazeeruddin, Adv. Funct. Mater. **28**, 1704351 (2018)
23. C. Yin, J. Lu, Y. Xu, Y. Yun, K. Wang, J. Li, L. Jiang, J. Sun, A.D. Scully, F. Huang, J. Zhong, J. Wang, Y.B. Cheng, T. Qin, W. Huang, Adv. Energy Mater. **8**, 1 (2018)
24. N. Berton, R. Nakar, B. Schmaltz, Synth. Met. **252**, 91 (2019)
25. G. Sathiyan, E.K.T. Sivakumar, R. Ganesamoorthy, R. Thangamuthu, P. Sakthivel, Tetrahedron Lett. **57**, 243 (2016)
26. D. Magaldi, M. Ulfa, M.P. Nghiêm, G. Sini, F. Goubard, T. Pauporté, T.T. Bui, J. Mater. Sci. **55**, 4820 (2020)
27. Y. Ko, Y. Kim, C. Lee, Y. Kim, Y. Jun, ACS Appl. Mater. Interfaces **10**, 11633 (2018)
28. V. Mimaite, J.V. Grazulevicius, R. Laurinaviciute, D. Volyniuk, V. Jankauskas, G. Sini, J. Mater. Chem. C **3**, 11660 (2015)
29. Y.S. Kwon, J. Lim, H.-J. Yun, Y.-H. Kim, T. Park, Energy Environ. Sci. **7**, 1454 (2014)
30. T. Leijtens, T. Giovenzana, S.N. Habisreutinger, J.S. Tinkham, N.K. Noel, B.A. Kamino, G. Sadoughi, A. Sellinger, H.J. Snaith, ACS Appl. Mater. Interfaces **8**, 5981 (2016)
31. T. Zhu, J. Su, F. Labat, I. Ciofini, T. Pauporté, ACS Appl. Mater. Interfaces **12**, 744 (2020)
32. P. Wang, M. Ulfa, T. Pauporté, J. Phys. Chem. C **122**, 1973 (2018)
33. P. Wang, Z. Shao, M. Ulfa, T. Pauporté, J. Phys. Chem. C **121**, 9131 (2017)
34. B. Viana, T. Pauporte, P. Wang, M. Ulfa, Z. Shao, Proc. SPIE **10533**, 105332R (2018)
35. F. Lamberti, T. Gatti, E. Cescon, R. Sorrentino, A. Rizzo, E. Menna, G. Meneghesso, M. Meneghetti, A. Petrozza, L. Franco, Chem **5**, 1806 (2019)